Light Metals 2015
Edited by: Margaret Hyland
TMS (The Minerals, Metals & Materials Society), 2015

CHEMICAL CHARACTERIZATION AND THERMODYNAMIC INVESTIGATION OF ANODE CRUST USED IN ALUMINUM ELECTROLYSIS CELLS

François Allard[1], Martin Désilets[1], Marc LeBreux[1], Alexandre Blais[2]
[1]Université de Sherbrooke; 2500 Boulevard de l'Université; Sherbrooke, Qc, J1K 2R1, Canada
[2]Rio Tinto Alcan (Arvida Research and Development Centre); 1955 Boulevard Mellon; Jonquière, Qc, G7S 4K8, Canada

Keywords: Aluminum electrolysis, Crust, Anode cover material, X-ray diffraction, Thermodynamic, Alumina

Abstract

The anode cover material (ACM) is necessary to control the top heat losses of aluminum electrolysis cells, to decrease the fluoride fumes emissions and to prevent air burn of carbon anodes. In order to understand the behavior of the ACM and anode crust at operating conditions, samples of these materials are taken from an industrial electrolysis cell in the side channel, center channel and between anodes. Their chemical compositions are analyzed by X-ray diffraction while the temperatures inside the crust are validated by temperature measurements. The reactions occurring in the ACM and anode crust are then determined by thermodynamic equilibrium calculations. Concentration gradients of chiolite ($Na_5Al_3F_{14}$), cryolite (Na_3AlF_6), $Na_2Ca_3Al_2F_{14}$, and Al_2O_3 are observed in the anode crust, implying a variation of the cryolite ratio and melting temperature of the crust. The thermodynamic analysis describes the state and behavior of the anode crust in aluminum electrolysis cells.

Introduction

The Hall-Héroult process can be improved through a better understanding of the chemical composition and behavior of the anode cover material (ACM) and anode crust. These materials are necessary to control the top heat losses of aluminum electrolysis cells, to decrease the fluoride fumes emissions and to prevent air burn of carbon anodes. The ACM is usually composed of recycled crushed bath and alumina. The granulometry is characterized by a mix of fine to coarse particles. At each anode change, the ACM is deposited over the anode. The anodes are replaced typically after a few weeks. This frequency varies depending on the cell technology and the rate of consumption of the carbon anode. The anode consumption is proportional to the current used in the process. Figure 1 depicts the main components of an industrial electrolysis cell.

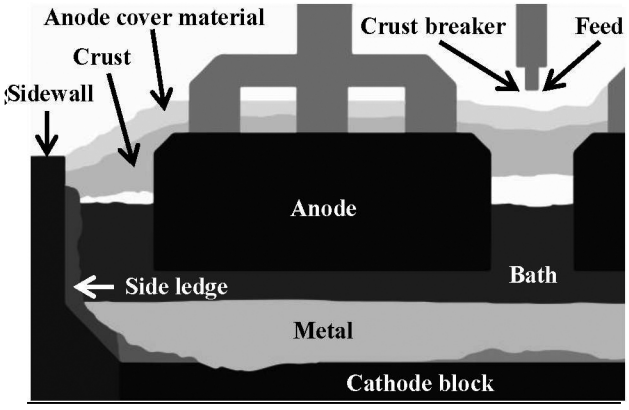

Figure 1. Schematic of an aluminum electrolysis cell.

The formation of anode crust was studied by several researchers in the last decades. Firstly, laboratory experiments have been conducted with alumina based ACM in order to study the mechanism of formation [1, 2, 3 ,4]. According to Less, the fluorides from the bath act as "mineralizers" and increase the conversion rate of γ-Al_2O_3 to α-Al_2O_3 [4]. He demonstrated the crusting behavior of alumina added in a cell with a standard cryolite melt. A low calcination temperature of the ore or a high content in γ-Al_2O_3 helps to form a strong crust due to the formation of a network between the α-Al_2O_3 particles. The crust formation is reduced when the ore has already reacted with bath fumes or when the alumina is mainly composed of fines particles [2]. The interaction of the bath with the alumina added on a cell was investigated by Gerlach and Winkhaus [5]. The bath penetrates into the alumina powder by capillary forces implying the formation of a crust consisting of solidified bath and embedded alumina particles.

The chemical composition of the crust taken from industrial cells has been investigated in a few studies [6,7,8]. Liu et al. observed the temperature profiles inside the side channel crust and determined the chemical composition by elemental analysis and by the wet chemistry method [8]. They demonstrated the gradient of AlF_3 in excess in the crust and the existence of liquid bath at temperature above 740 °C. More recently, Groutso et al. showed the gradient of chiolite in the crust with X-ray diffraction analysis [7]. The chemical composition of anode crust made from crushed bath mixed with alumina was demonstrated by Zhang et al. [6]. They revealed the development of porosity in the crust, thus allowing the penetration of bath and fumes. The crust in industrial cells has a vertical gradient of cryolite ratio (CR). The bottom is more concentrated in cryolite and the top zone is more acidic [6].

In the present study, samples of crust were collected in the side channel, between anodes and in the center channel. The chemical composition of each sample was determined by the Rietveld method performed on X-ray diffraction results. The reactions occurring in the ACM and crust were predicted by thermodynamic equilibrium calculations based on the temperatures measured in the crust. The thermodynamic studies help to understand the behavior of the crust and predict the melting temperatures of the phases inside the crust.

Methodology

Some samples were collected in an industrial cell in order to understand the anode crust chemical composition and behavior. Moreover, the temperature inside the crust of the side channel was measured throughout the life of the anode. The samples were taken at three different locations around the anode: 1) side channel, 2) between the anodes, and 3) center channel (Figure 2).

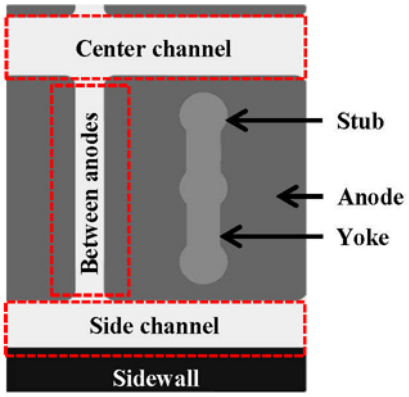

Figure 2. Position of the crust samples collected in the industrial cell (top view).

Firstly, three samples were taken before anode replacement, i.e. at the end of life of the anode. Secondly, three other samples were taken after the temperature measurements, also at the end of life of the anode. Thus, two sets of samples were collected for each position. The granular ACM used to cover the anode before the temperature measurements was also sampled. Finally, each sample was characterized in order to obtain their chemical compositions.

Characterization of the ACM and Crust Samples

Each sample of crust was cut in such a way to study the vertical concentration gradients. Afterward, the sample was ground in fine powder using a ball mill for X-ray diffraction (XRD) and oxygen analysis. A diffraction pattern of the crystalline phases in the sample was obtained with the XRD. The XRD data were also analyzed with a Rietveld method to obtain the chemical composition. The Al_2O_3 concentration was determined by oxygen measurement (LECO).

X-Ray Diffraction (XRD). A PANalytical X'Pert PRO MPD diffractometer was used to obtain the diffraction pattern of the samples. The rotation speed of the sample holder was set to 1 s^{-1} and the data were obtained with the Cu Kα X-ray radiation. The diffraction pattern was acquired by using a PIXcel^{1D} detector. The XRD data were collected from 10° to 74° at a 2θ angle with a resolution of 0.0263° and a time of 0.12 s per step.

Oxygen Measurement. The oxygen content was determined using a TCH-600 (LECO) in order to calculate the Al_2O_3 in each sample. The samples were each placed inside a nickel capsule and were analyzed in triplicate. This method is useful to quantify the crystalline and amorphous phases of Al_2O_3 in the sample assuming that all the oxygen detected comes from Al_2O_3.

Scanning Electron Microscopy (SEM). Some samples of crust were observed with a Hitachi S-4700 SEM. The elemental composition was evaluated with an Oxford X-Max 50 mm^2 energy dispersive X-ray spectroscopy (EDS) module. The analyses were conducted at an acceleration voltage of 20 kV, an intensity of the beam of 10 µA and a working distance of 12 mm.

Rietveld Quantification. The crystalline phases in the various samples were quantified with a Rietveld method performed on XRD data. The Rietveld refinements were obtained with the software PANalytical HighScore Plus. The following phases were selected for the quantification: Na_3AlF_6, $Na_5Al_3F_{14}$, $NaAlF_4$, $Na_2Ca_3Al_2F_{14}$, $NaCaAlF_6$, $Na_4Ca_4Al_7F_{33}$, CaF_2, NaF, AlF_3, α-Al_2O_3, γ-Al_2O_3, δ-Al_2O_3, θ-Al_2O_3, β-Al_2O_3, Al_4C_3, Al and C. The chemical composition of each sample discussed in this article is expressed in weight percentage. The CR of the sample is the molar ratio of NaF/AlF_3 and is calculated with the stoichiometric concentration of compounds as determined by the Rietveld method.

Amorphous Quantification. Each XRD analysis was conducted on powdered samples and on samples mixed with an internal standard of quartz (99.5 % SiO_2). The amorphous content was completed by adding 20 % of quartz in the sample. Equation 1 was used to determine the amorphous fraction in the quartz doped samples.

$$w_{amorphous} = \frac{1}{1 - w_1} - \frac{w_1}{w_2(1 - w_1)} \quad (1)$$

Where $w_{amorphous}$ is the mass fraction of the amorphous content in the sample, w_1 is the mass fraction of the quartz added (20 %) and w_2 is the mass fraction of quartz as determined by the Rietveld method. The amorphous content gives the fraction of the sample which could not be detected with the XRD.

Thermodynamic Investigation

The thermodynamic equilibrium analysis was based on the results of Rietveld quantification and the Al_2O_3 concentration obtained by oxygen measurement. This investigation helped to describe the behavior of the ACM and the crust in industrial electrolysis cells. The reactions in the crust and the temperatures of phase transitions were calculated using the FactSage software (version 6.4). FactSage calculates the thermodynamic equilibrium based on the minimization of Gibbs free energy [9]. The NaF-AlF_3-CaF_2-Al_2O_3 system was modeled with the FTHall database. The thermodynamic equilibrium calculations were carried out at atmospheric pressure.

Results and Discussion

To investigate the crust chemical composition, samples of crust were taken at the end of life of two anodes. During the anode replacement, samples were collected in the side channel (SC), in the center channel (CC) and between the anodes (BA). After the anode change and before adding the ACM, the liquid bath was in contact with air. The top part of bath froze quickly. A sample of this freeze was collected before adding the ACM. Some thermocouples were placed in the side channel in order to verify the temperature of the ACM and crust during the life of the anode. A set of samples was taken before the temperature measurements and another set after the temperature measurements, both at the end of life of the anodes. The chemical compositions of the ACM and crust samples are described in the Table 1.

Table 1. Chemical Compositions of the ACM and Crust Samples

Sample	Height* (mm)	Na_3AlF_6 (%)	$Na_5Al_3F_{14}$ (%)	AlF_3 (%)	$Na_2Ca_3Al_2F_{14}$ (%)	$NaCaAlF_6$ (%)	α-Al_2O_3 (%)	T-Al_2O_3** (%)	Amorph. Al_2O_3 (%)	Other (%)	Amorph. (%)	Total Al_2O_3 (%)	CR
ACM	-	7.4	12.2	0.9	1.6	0.5	26.3	30.0	19.9	1.2	35.8	76.2	1.82
Freeze	-	58.0	29.5	0.4	4.8	3.3	1.7	0.6	0.0	1.7	23.2	2.3	2.29
SC-before	0-45	79.9	10.9	0.0	5.0	2.7	0.5	0.1	0.0	0.9	34.3	0.6	2.64
	45-90	80.0	10.8	0.0	5.3	2.6	0.6	0.0	0.0	0.7	49.7	0.6	2.65
	90-125	85.1	7.6	0.0	4.1	2.2	0.1	0.0	0.0	0.9	40.0	0.1	2.72
	125-160	85.5	7.4	0.0	3.8	1.7	0.1	0.0	0.0	1.5	40.2	0.1	2.76
BA-before	0-22	14.8	38.7	1.0	3.6	0.0	41.4	0.0	0.0	0.5	27.4	41.4	1.84
	22-44	11.2	45.1	1.2	2.1	0.0	39.8	0.0	0.0	0.6	34.1	39.8	1.77
	44-66	4.5	42.4	2.0	1.4	0.0	38.3	2.5	4.5	4.4	42.3	45.3	1.55
CC-before	0-32	37.6	17.2	0.6	10.3	1.4	31.5	0.5	0.0	0.9	34.0	32.0	2.20
	32-64	9.9	44.7	1.0	4.3	1.2	34.9	3.5	0.0	0.5	32.5	38.4	1.73
	64-96	2.3	53.8	1.5	0.9	0.0	26.2	5.5	9.0	0.8	25.3	40.7	1.61
SC-after	0-50	1.4	50.9	3.8	1.0	1.2	37.0	0.5	0.0	4.2	50.8	37.5	1.43
	50-100	2.4	39.4	7.2	0.9	1.0	45.4	0.8	0.0	2.9	44.8	46.2	1.27
	100-150	8.0	27.0	3.5	0.7	0.7	54.7	4.3	0.0	1.1	36.6	59.0	1.57
BA-after	0-5	80.6	10.3	0.0	4.5	2.0	0.4	0.1	0.0	2.1	23.7	0.5	2.67
	5-16	38.7	19.8	0.0	7.6	0.0	31.9	1.0	0.0	1.0	41.9	32.9	2.29
	16-32	27.6	30.6	0.7	6.5	0.0	34.0	0.0	0.0	0.6	37.2	34.0	2.05
	32-48	7.3	49.9	2.7	1.4	0.7	21.4	4.3	10.4	1.9	32.8	36.1	1.60
	48-53	1.4	37.5	6.2	1.3	0.0	9.7	10.7	28.9	4.3	19.0	49.3	1.29
CC-after	0-11	31.2	25.9	0.0	7.8	2.7	31.4	0.6	0.0	0.4	35.0	32.0	2.12
	11-22	21.3	37.6	0.5	3.0	0.0	36.7	0.8	0.0	0.1	51.1	37.5	1.98
	22-33	3.3	56.8	2.4	1.2	0.4	23.6	4.9	6.1	1.3	29.3	34.6	1.57
	33-41	2.3	36.6	4.9	0.6	0.0	7.9	10.2	34.5	3.0	15.0	52.6	1.36

* Position from the bottom to the top of the sample; ** T-Al_2O_3 is the sum of the Al_2O_3 transition phases (γ, δ, θ, β)

The main crystalline phases detected by XRD are described in Table 1 (Na_3AlF_6, $Na_5Al_3F_{14}$, AlF_3, $Na_2Ca_3Al_2F_{14}$, $NaCaAlF_6$, α-Al_2O_3). T-Al_2O_3 is the sum of each transition phase of alumina detected by XRD (γ, δ, θ, β). The column "Other" includes the following phases: $NaAlF_4$, $Na_4Ca_4Al_7F_{33}$, CaF_2, Aluminum, and Carbon. The amorphous fraction of Al_2O_3 was labeled "Amorph. Al_2O_3". The column "Amorph." is given as an indication. It describes the part of the sample which could not be quantified by XRD (without considering Al_2O_3). The "Total Al_2O_3" is the Al_2O_3 content determined by oxygen analysis.

Composition of the Industrial Samples

ACM Sample. The ACM is made of recycled anode cover, crushed bath and alumina. It was added around the anode in order to form the crust which was studied by temperature measurements. The ACM sample showed a high content of Al_2O_3 composed of 30.0 % of Al_2O_3 transition phases (γ, δ, θ, β), 19.9 % of amorphous Al_2O_3 and 26.3 % of stable α-Al_2O_3. The ACM contained a low concentration of calcium species and Na_3AlF_6 compared to the freeze above the bath. The CR of the ACM added around the anode (1.82) was lower than the CR of the freeze formed above the bath (2.29).

Side Channel Samples. The chemical composition of each sample varied depending on the nature of the sample and on the position in the cell. Regular operations were maintained during the life of the studied anodes. Firstly, the sample collected in the side channel before the temperature measurements (SC-before) had a similar chemical composition to the ledge on the sidewall. The anode cover was thin in this region and thus the sample was taken on the top of the side ledge. The sample was white and the texture was more like crystals. It was also irregular compared to the other samples of anode crust. Moreover, the CR was very high (2.64 to 2.76) and the Al_2O_3 concentration was low (0.6 to 0.1 %). The appearance of the sample SC-after was similar to the other samples of crust taken in the CC and BA. This sample did not demonstrate a clear vertical gradient of CR or acid species. The middle and the bottom of the sample SC-after were very acidic. The XRD analysis demonstrated a concentration of $Na_4Ca_4Al_7F_{33}$, a very acid species. Concentrations of 3.5 % and 1.2 % were detected in the bottom and the middle of the sample. $Na_4Ca_4Al_7F_{33}$ was only detected in this sample, and was included in the column "Other". Results showed also the presence of a vertical gradient of Al_2O_3. The top of the sample was more concentrated in Al_2O_3 than the bottom (59.0 % to 37.5 %). The CR of the sample was lower than the ACM. The same trend was observed with the Al_2O_3 concentration.

Samples Between Anodes. The samples taken between anodes showed clearly the vertical gradients of Na_3AlF_6, $Na_5Al_3F_{14}$, AlF_3, $Na_2Ca_3Al_2F_{14}$, and Al_2O_3. The bottom part of theses samples contained more Na_3AlF_6 and $Na_2Ca_3Al_2F_{14}$. The top part contained more $Na_5Al_3F_{14}$, AlF_3, and Al_2O_3. At the beginning of the crust formation, the liquid bath penetrates by capillary forces in the ACM to form crust [5]. The penetration of the bath in the ACM increased the content in $Na_2Ca_3Al_2F_{14}$ and Na_3AlF_6 in the bottom part of the sample. The top part of the sample BA-after (48-53 mm) also showed a concentration of $NaAlF_4$ (2.3 %) according to XRD. The top of the sample BA-after had a very low CR (1.29). Both samples BA showed a vertical gradient of CR.

Center Channel Samples. The samples collected at the CC had similar chemical compositions than the samples located BA. They demonstrated a significant concentration gradient of acid species ($Na_5Al_3F_{14}$, AlF_3), calcium cryolite ($Na_2Ca_3Al_2F_{14}$), Na_3AlF_6 and Al_2O_3. The concentration gradient of $Na_2Ca_3Al_2F_{14}$ was more important in the CC crust compared to the crust BA. A concentration of $NaAlF_4$ (1.7 %) was also detected in the sample CC-after (33-41 mm) and its CR was also very low (1.36).

Al_2O_3 in the Crust. The samples of anode crust investigated in this study showed a vertical gradient of Al_2O_3. Moreover, the Al_2O_3 at the bottom part of the crust had a higher fraction of α-Al_2O_3 than the top. The top of the crust contained more T-Al_2O_3 (γ, δ, θ, β) and amorphous Al_2O_3. The bottom of the crust had a higher temperature as it is closer to the bath. According to Less, a higher temperature and a contact with fluoride vapor increase the conversion of the transition phases of Al_2O_3 to the stable alpha phase [4]. The samples SC-after (50-100 mm) and CC-after (11-22 mm) were observed by SEM-EDS (Figures 3 and 4).

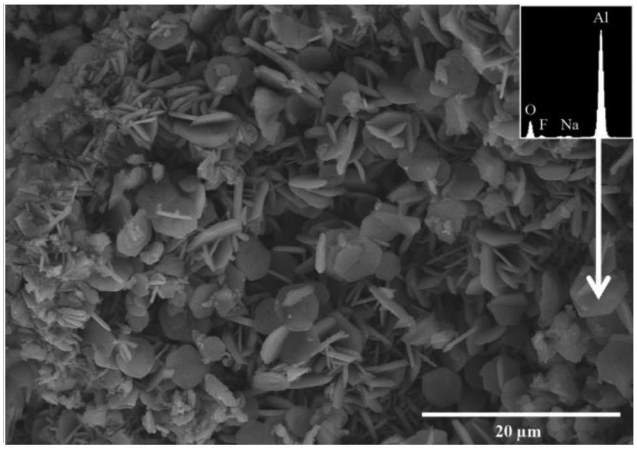

Figure 3. Alumina platelets in the sample SC-after (50-100 mm).

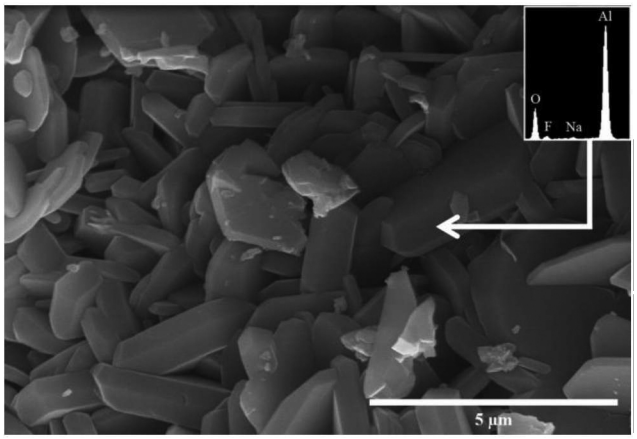

Figure 4. Alumina platelets in the sample CC-after (11-22 mm).

Figure 3 was taken at a magnification of 2000 x and Figure 4 at 10 000 x. The Al-O content in the platelets was demonstrated by elemental analysis (EDS). Thus, both figures show the network of α-Al_2O_3 inside the crust. The α-Al_2O_3 particles consolidate together in order to form a network, thus increasing the strength of the crust [2]. The solid bath around the particles also increases the strength of the crust [8]. SEM-EDS analysis of the crust also showed areas where the hexagonal Al_2O_3 particles are embedded by solid bath.

Temperature Measurements in the Crust

The temperature evolving in the SC was evaluated in order to investigate the reactions occurring in the ACM and crust. The thermocouples (type K with Inconel sheath) were positioned following the installation of the new anode. Afterward, the SC was covered with the ACM. The bottom thermocouple (T_1) was placed on the surface of the top freeze, T_2 was located in the middle of the ACM in the SC and T_3 was close to the top. Figure 5 depicts the location of the thermocouples and Figure 6 shows the temperature measurements in the SC.

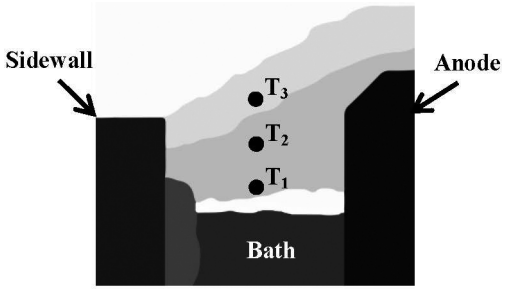

Figure 5. Location of the thermocouples in the SC.

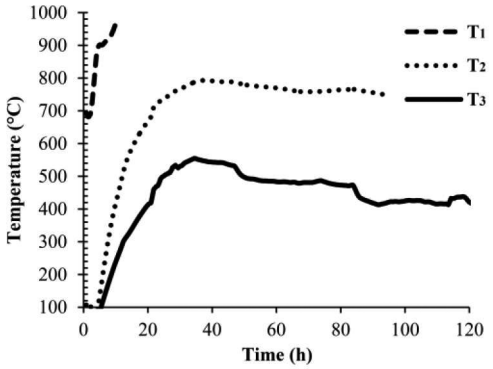

Figure 6. Temperature measurements in the SC crust.

The temperature in the bottom of the crust increased quickly. After 10 hours, it reached 970 °C and the thermocouple became unstable. At this temperature, the top freeze under T_1 melted and the liquid bath likely corroded the thermocouple. Liquid bath is very aggressive for any metallic instruments, even with an Inconel sheath. The temperature of T_2 reached 792 °C after 40 hours and it began to decrease over the time. T_3 also got to a maximum after 40 hours (555 °C). The reactions in the ACM and crust as a function of the temperature are described by the thermodynamic investigation.

Thermodynamic Investigation of Industrial Anode Crust

The behavior of the ACM and crust in an industrial cell is described by thermodynamic equilibrium calculations. The NaF-AlF_3-CaF_2-Al_2O_3 system, supersaturated in Al_2O_3, describes the reactions occurring in the ACM and crust. The temperature of phase transitions varied significantly depending on the cryolite ratio. Figure 7 shows the phase diagram of anode crust in industrial cells. The concentration of Al_2O_3 and CaF_2 was kept at 40 % and 2 % respectively in order to reproduce the typical chemical composition of the crust.

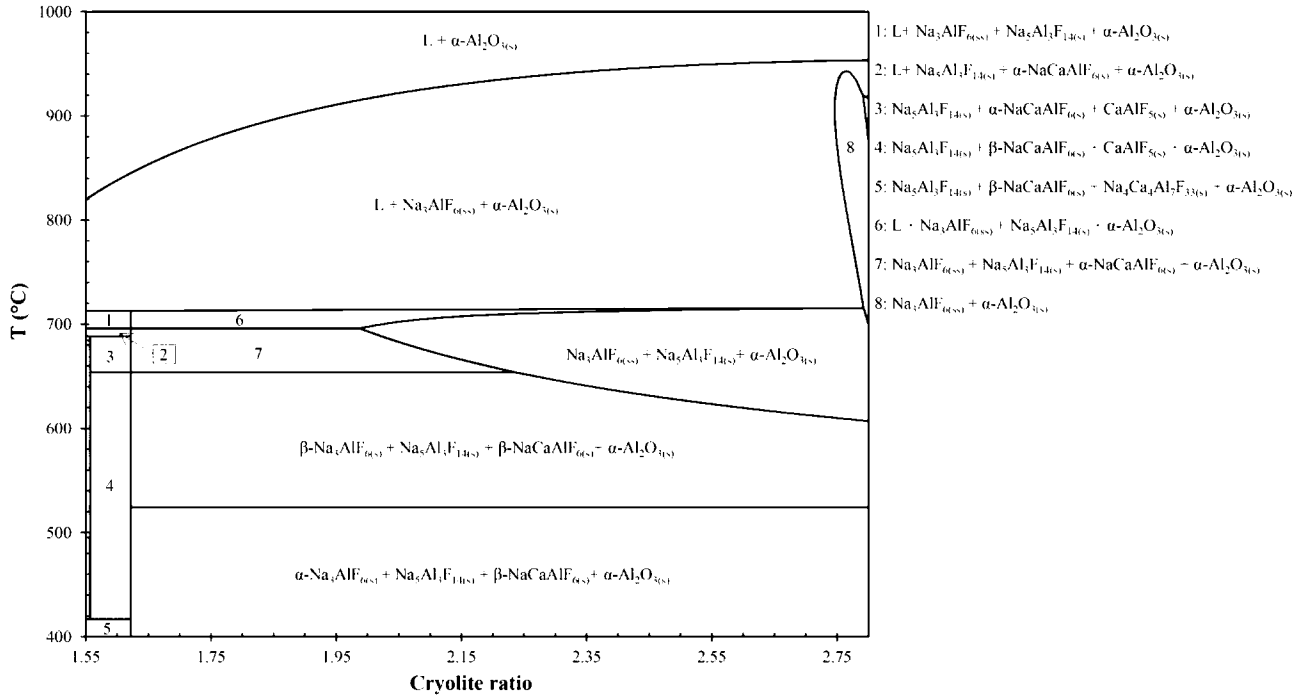

Figure 7. Phase diagram of the crust depending on the cryolite ratio (Al_2O_3 = 40 % and CaF_2 = 2 %).

Reactions in the ACM and Crust. A wide range of temperatures was measured in the crust. The phase diagram (Figure 7) demonstrates the behavior of the crust at temperature between 400 °C to 1000 °C. At low temperature, the crust contains Na_3AlF_6, $Na_5Al_3F_{14}$, $NaCaAlF_6$, and Al_2O_3, at CR between 1.62 and 2.80 and at thermodynamic equilibrium conditions. The conversion of the Na_3AlF_6, from alpha to beta, occurs at a temperature of 524 °C.

$$\alpha - Na_3AlF_{6(s)} \rightarrow \beta - Na_3AlF_{6(s)} \qquad (1.62 < CR < 2.80)$$

The crust of CR < 1.62 is composed by $Na_5Al_3F_{14}$, $NaCaAlF_6$, $Na_4Ca_4Al_7F_{33}$, and Al_2O_3 at a temperature below 417 °C. The acidic calcium cryolite, $Na_4Ca_4Al_7F_{33}$, was detected in the sample SC-after. The crust begins to melt at temperature of 696 °C due to the presence of $NaCaAlF_6$ (1.62 < CR < 2.0). At the same temperature, $NaCaAlF_6$ is dissolved in the Na_3AlF_6 solid solution at CR > 2.0. Na_3AlF_6 is produced at CR < 1.62 due to the melting of $NaCaAlF_6$ and $Na_5Al_3F_{14}$. The thermodynamic analysis shows a small concentration of stable $NaCaF_5$ between 417 °C and 688 °C (1.56 < CR < 1.62). $NaCaF_5$ melts at a temperature of 688 °C.

Excluding Al_2O_3, the major part of the crust is composed of $Na_5Al_3F_{14}$. The incongruent melting of the $Na_5Al_3F_{14}$ varies slightly depending on the CR. This compound melts at 713 °C and 715 °C with a CR of 1.55 and 2.79 respectively. At CR < 1.37, the $Na_5Al_3F_{14}$ melts completely at 712 °C, without producing Na_3AlF_6.

$$Na_5Al_3F_{14(s)} \rightarrow L + Na_3AlF_{6(s)} \qquad (1.37 < CR < 2.79)$$
$$Na_5Al_3F_{14(s)} \rightarrow L \qquad (CR < 1.37)$$

The $Na_5Al_3F_{14}$ content also decreases with increasing CR. The liquid fraction in the sample is very low at high CR. At CR around 2.8, the melting begins at a temperature of 920 °C. A lower CR also decreases the melting temperature of the Na_3AlF_6. Na_3AlF_6 completely melts at 953 °C with CR of 2.8 and 818 °C with CR of 1.55. Industrial crust of CR < 1.37 does not contain Na_3AlF_6 at any temperature and the bath phases completely melt at 712 °C. The main phase transitions occurring in the industrial samples of ACM and crust are described in Table 2. $T_{Na5Al3F14}$ and $T_{Na3AlF6}$ are the melting temperatures of the corresponding compounds.

Table 2. Summary of the Main Phase Transitions in the ACM, Freeze and Crust

Sample	Height (mm)	CR	$T_{Na5Al3F14}$ (°C)	$T_{Na3AlF6}$ (°C)
ACM	-	1.82	709	892
Freeze	-	2.29	714	970
SC-before	0-45	2.64	715	993
	45-90	2.65	715	994
	90-125	2.72	716	1000
	125-160	2.76	717	1002
BA-before	0-22	1.84	714	895
	22-44	1.77	717	878
	44-66	1.55	717	807
CC-before	0-32	2.20	700	928
	32-64	1.73	711	875
	64-96	1.61	719	824
SC-after	0-50	1.43	711	762
	50-100	1.27	702	-
	100-150	1.57	714	826
BA-after	0-5	2.67	716	997
	5-16	2.29	709	937
	16-32	2.05	711	921
	32-48	1.60	717	830
	48-53	1.29	704	-
CC-after	0-11	2.12	704	925
	11-22	1.98	716	915
	22-33	1.57	718	-
	33-41	1.36	713	-

In the samples, $Na_5Al_3F_{14}$ melts at temperatures between 700 °C and 719 °C depending on the CR and CaF_2 content. The CaF_2 decreases the melting temperature of $Na_5Al_3F_{14}$ according to thermodynamic equilibrium calculations. Na_3AlF_6 begins to melt from $T_{Na5Al3F14}$ and finishes to melt at $T_{Na3AlF6}$. Thus, this compound melts gradually between ~700 °C and ~1000 °C in the anode crust, depending on the chemical composition. The gradient of CR in the crust implies a variation in the melting temperature of the bath phases present in the crust. The higher part of the crust has more risk to collapse compared to the bottom due to its lower CR. If the temperature reaches 700 °C, most of the bath phases, in the middle and top of the crust, would be in liquid state. In this condition, the crust is only supported by the Al_2O_3 platelets.

Behavior of the Crust in Industrial Cells. At the beginning of anode life, the SC was filled with ACM deposited on a thin layer of freeze. Due to the insulating effect of ACM, this freeze begins to melt at 714 °C and finishes to melt at 970 °C according to thermodynamic calculations (Table 2). Thus the bottom of the crust, initially composed by frozen bath, melts after 10 hours, when it reaches a temperature of 970 °C (Figure 6). The thermodynamic analysis demonstrated the presence of liquid phases in the ACM and crust due to the acidic phases detected by XRD ($Na_5Al_3F_{14}$, $Na_2Ca_3Al_2F_{14}$, $NaCaAlF_6$, $Na_4Ca_4Al_7F_{33}$, and $NaAlF_4$). The liquid phase appears in the ACM at a temperature of 696 °C due to the $NaCaAlF_6$ content. The melting of $Na_5Al_3F_{14}$ occurs at 709 °C and melting of Na_3AlF_6 finishes at 892 °C. Consequently, the consolidation of the ACM into crust is initiated at a temperature of 696 °C due to the liquid species inside the ACM. Moreover, the weakness of the crust increases with a higher content of liquid. Thus, a highly acidic crust has more risk to collapse. For instance, a crust of CR < 1.37 will be only supported by the α-Al_2O_3 network if its temperature reaches 712 °C (2 % of CaF_2), as all acidic compounds melt at this temperature.

Formation of the Crust. The formation of crust begins with the penetration of liquid bath in the ACM at the beginning of anode life [5]. This process is also achieved when the $NaAlF_4$ vapor coming from the bath fumes diffuses into the ACM [8]. $NaAlF_{4(g)}$ freezes in the ACM and decomposes to form $Na_5Al_3F_{14(s)}$ and $AlF_{3(s)}$. According to thermodynamic analysis, $NaAlF_4$ freezes at a temperature of 685 °C. Consequently, the temperature must be higher than 685 °C to form crust. Otherwise, the $NaAlF_4$ will be solid and no liquid phase will favor the consolidation of the crust. The top of the crust in industrial samples did not completely transform into stable α-Al_2O_3, as the temperature was not sufficient. The liquid in the ACM increases the conversion of the transition phases of Al_2O_3 (γ, δ, θ, β) to stable α-Al_2O_3. In this process, the α-Al_2O_3 platelets cement together and grow to form a strong network.

Industrial Implications of the Results. The melting temperatures of the phases in the industrial crust are strongly influenced by the gradients of acid species. The bottom of the crust is less acidic (CR close to the bath) and the top is highly acidic. While the electrolysis cell is in operation, the liquid bath splashes on the bottom of the crust, thus causing partial melting of the crust and forming stalactite crystal as observed by Zhang et al. [6]. Bath vapor, mainly composed of $NaAlF_4$, also diffuses in the crust. As detected by XRD, this increases the content in acid species over time, making the crust more vulnerable to collapse. Moreover, the vapor pressure of $NaAlF_4$ increases with temperature [10]. Consequently, a higher quantity of $NaAlF_4$ will diffuse in the crust when the bath is at a higher local temperature. Thus, high bath temperature and frequent anode effects are detrimental to the stability of the crust. At plant scale, the acidity of the ACM could also increase over time, as the ACM is made from recycled crust. Additionally, $NaAlF_4$ vapor and bath splashes which penetrate in the crust contain a low Al_2O_3 concentration, thereby reducing its concentration in the crust. The crust made from ACM with a lower CR and lower Al_2O_3 presents a higher risk to collapse, thus amplifying operational problems. The crust is supersaturated in Al_2O_3 and it may sink into the bath leading to sludge formation.

Conclusions

The Rietveld method applied to X-ray diffraction results demonstrated the existence of vertical gradients of $Na_5Al_3F_{14}$, Na_3AlF_6, $Na_2Ca_3Al_2F_{14}$, and Al_2O_3 in the crust taken in the center channel and between anodes. Only a gradient of Al_2O_3 was found in the side channel. The top of the crust also showed a concentration of amorphous Al_2O_3 and transition phases of Al_2O_3, while the bottom was crystalline. An acidic crust is more likely to melt or collapse due to a lower melting temperature. Thermodynamic analysis demonstrated that the melting temperature of the crust is 712 °C when the CR is less than 1.37. The presence of liquid phase in the crust is due to the concentration of $Na_5Al_3F_{14}$, $Na_2Ca_3Al_2F_{14}$, $NaCaAlF_6$, $Na_4Ca_4Al_7F_{33}$, and $NaAlF_4$. The consolidated crust is weakened by the bath vapor, by splashing of the bath and by a high content of acid species.

Acknowledgements

This work is financed and supported by Rio Tinto Alcan, "Conseil de Recherches en Sciences Naturelles et en Génie du Canada" (CRSNG) and "Fonds de Recherche du Québec - Nature et Technologies" (FRQNT).

References

1. R. Oedegard et al., "On Alumina Phase Transformation and Crust Formation in Aluminum Cells," *Light Metals*, 1985, 695-709.
2. D.W. Townsend and L.G. Boxall, "Crusting Behavior of Smelter Aluminas," *Light Metals*, 1984, 649-665.
3. T.J. Johnston and N.E. Richards, "Correlation Between Alumina Properties and Crusts," *Light Metals*, 1983, 623-639.
4. L.N. Less, "The Crusting Behavior of Smelter Aluminas," *Metallurgical Transactions B*, 8 (1977), 219-225.
5. J. Gerlach and G. Winkhaus, "Interactions of Alumina with Cryolite-Based Melts," *Light Metals*, 1985, 301-313.
6. Q. Zhang et al., "Composition and Thermal Analysis of Crust Formed from Industrial Anode Cover," *Light Metals*, 2013, 675-680.
7. T. Groutso, M. Taylor, and A.K. Hudson, "Aspects of Crust Formation from Today's Anode Cover Material," *Light Metals*, 2009, 405-410.
8. X. Liu, M. Taylor, and S. George, "Crust Formation and Deterioration in Industrial Cells," *Light Metals*, 1992, 489-494.
9. P. Chartrand and A.D. Pelton, "A Predictive Thermodynamic Model for the Al-NaF-AlF_3-CaF_2-Al_2O_3 System," *Light Metals*, 2002, 245-252.
10. H. Kvande, "Vapour-phase studies of NaF-AlF_3 melts. 1. The AlF_3-rich part.," *High Temp. - High Pres.*, 15 (1983), 51-62.